Appl Nanosci (2014) 4:359–365
DOI 10.1007/s13204-013-0217-x

ORIGINAL ARTICLE

Synthesis and characterization of Ce^{3+}-doped flowerlike ZnS nanorods

N. Shanmugam · S. Cholan · G. Viruthagiri · R. Gobi · N. Kannadasan

Received: 25 January 2013 / Accepted: 20 March 2013 / Published online: 2 April 2013

Abstract Cerium-doped zinc sulfide nanorods with flower-shaped morphology have been successfully synthesized in air atmosphere through simple chemical precipitation method. The incorporation of Ce^{3+} was confirmed by X-ray diffraction and energy-dispersive spectrum. The doping of Ce^{3+} ions has significant influence on the optical properties of the synthesized rods. UV–Vis absorption spectroscopy measurements have shown that the absorption peak of doped ZnS was red shifted compared to undoped ZnS. Photoluminescence measurements reveal that luminescence intensity of Ce^{3+} was enhanced considerably by the energy transfer from ZnS. The existence of functional groups was identified using Fourier transform infrared spectrometer. Field emission scanning electron microscope results show a uniform growth pattern of the nanorods with flowerlike structure. High resolution transmission electron microscopy results showed that the doped ZnS nanocrystals are composed of uniform nanorods with average diameter of 22 nm and length of 140 nm. The thermal stability of the nanorods was confirmed using thermo gravimetric and differential thermal analysis.

Keywords ZnS nanorods · Flowerlike structure · FESEM · HRTEM · EDS

N. Shanmugam (✉) · S. Cholan · G. Viruthagiri · R. Gobi · N. Kannadasan
Department of Physics, Annamalai University, Annamalai Nagar, Chidambaram 608 002, Tamilnadu, India
e-mail: quantumgosh@rediffmail.com

Introduction

In the modern scientific era, optical properties of doped semiconductor nanoparticles have shown great impact as their electronic structure and electro magnetic fields are drastically modified due to quantum confinement effects. Tailoring the color output of nanomaterials has been playing an important role for their applications as light emitting displays, field emitters (Fang et al. 2007; Bando et al. 2007), lasers, sensors (Fang et al. 2009) and opto-electronic devices to multiplexed biological labeling (Torimoto et al. 2007; Yu et al. 2010). The luminescence properties of ZnS nanoparticles have been tuned by doping with varies transition metals and rare-earth metals (Manzoor et al. 2004; Hu and Zhang 2006; Kim 2009; Ageeth and Meijerink 2001). Since ZnS has wide band gap of 3.68 eV at room temperature, its nanocrystals are the suitable host materials for the doping elements such as RE and transition metal ions which are optically and magnetically active. Rare-earth ions are categorized by group of elements known as the lanthanides and are most stable in their triply ionized form. Furthermore, ZnS is one of the eco friendly materials, the RE-doped ZnS nanocrystals can be used in producing efficient phosphor materials with a gamut of colors (Bhargava 1996). ZnS host is able to produce red, blue, and green luminescence due to various RE ion dopants. So far, different synthesis routes have been suggested for the preparation of RE-doped ZnS nanorods under low temperature and in particular, the effect of dopant on the structures and optical properties are limited (Wang and Fan 2006). In this paper, we have attempted with a simple chemical precipitation method to prepare the Ce^{3+}-doped flower-shaped ZnS nanorods. From this method, cerium-doped nanorods of ZnS with flowerlike morphology have been obtained.

Experimental

Materials

Zinc acetate dihydrate [$Zn(CH_3COO)_2{\cdot}2H_2O$], thiourea [$NH_2CSNH_2$], cerium(III)chloride hepta hydrate[$(CeCl_3){\cdot}7H_2O$] were purchased from Merck. All chemicals were used as received since they were of analytical regent grade with 99 % purity. The glass wares used in this experimental work were acid washed. Ultrapure water was used for all dilution and sample preparation.

Synthesis of Ce^{3+}-doped ZnS nanorods and undoped ZnS nanocrystals

For the synthesis of Ce^{3+}-doped ZnS nanorods, 3 g (0.35 M) of zinc acetate [$Zn(CH_3COO)_2{\cdot}2H_2O$] in 40 ml of deionized water–ethanol matrix (equal volume) and an appropriate amount of cerium in 10 ml aqueous were mixed drop by drop. Then, 3 g (1 M) of thiourea [NH_2CSNH_2], in 40 ml of deionized water–ethanol matrix was added drop by drop to the above mixture. The entire mixture was stirred magnetically at 80 °C until the homogeneous solution was obtained. Finally, the product was dried in a hot air oven at 120 °C for 2 h. A similar method of preparation, without the addition of cerium, was used to synthesize undoped ZnS nanocrystals.

Characterization

The X-ray diffraction (XRD) patterns of the powdered samples were recorded using X′ PERT PRO diffractometer with Cu-K_α radiation ($\lambda = 1.5406$ Å). The crystallite size was estimated using the Scherrer equation. The optical absorption spectra of all the samples in deionized water were recorded using LAMDA 25 PERKIN ELMER spectrometer. Fluorescence measurements were performed on a VARIAN spectrophotometer. The FT-IR spectra were recorded from a SHIMADZU-8400 spectrometer using KBr pellet technique. The morphology of the product was observed by a HITACHI S-4700 field emission scanning electron microscope (FESEM). Energy-dispersive spectrum (EDS) measurement was carried out with the EDS arrangement enclosed with HITACHI S-4700 FESEM. High-resolution transmission electron microscopy (HRTEM) analysis was performed using JEOL 3010 HRTEM to study the morphology and size of the nanocrystals. Thermo gravimetric analysis (TGA) and differential thermal analysis (DTA) studies have been performed using Perkin Elmer Diamond TGA/DTA instrument at a heating rate of 20 °C/min in air.

Result and discussion

XRD-analysis

Figure 1 shows the XRD patterns of ZnS and cerium-doped ZnS samples. The XRD patterns of both undoped and cerium-doped ZnS have three main diffraction features corresponding to (111), (220), and (311) planes and all the three peaks can be indexed to standard cubic ZnS (JCPDS card No-05-0566). No reflections related to Ce^{3+} ions and other impurities were identified in the pattern, indicating the high purity of the final product. The three peaks of the XRD patterns of cerium-doped ZnS clearly show shifting of the center of the diffraction peaks slightly toward the lower angle on Ce^{3+} doping in comparison to that of pure ZnS. Moreover, the obtained reflections are sharp and high in intensity which reveals that the synthesized nanorods are well crystalline. In addition, the lattice constants of Ce^{3+}-doped ZnS ($a = 5.486$ Å) were found to be slightly larger than those to pure ZnS ($a = 5.406$ Å). This is consistent with the fact that the ionic radius of Ce^{3+} is 1.03 Å whereas that of Zn^{2+} is 0.74 Å. The shifting of XRD lines with doping simply suggest that Ce^{3+} was successfully substituted into the ZnS host structure at the Zn^{2+} site. The size of the nanocrystals was determined from the schrerrer formula $D = 0.9\lambda/\beta\cos\theta$, where D is the crystallite size, λ is the wavelength of the incident X-ray (1.54 Å), θ is the Bragg's angle and β is the full width at half maximum (FWHM). From the X-ray line broadening the crystallite sizes of ZnS and Ce^{3+}-doped ZnS are estimated around 5.3 and 22 nm ($r = \pm 10$ %), respectively. Such an increase in particle size is clearly evident from the Fig. 1 that the broadening of diffraction peaks decreased on cerium doping.

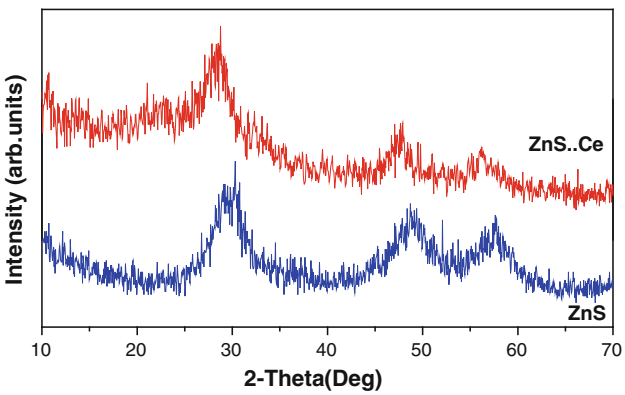

Fig. 1 X-ray diffraction patterns of ZnS and Ce^{3+}-doped ZnS nanorods

Optical absorption studies

UV–visible absorption analysis is a useful method for the characterization of semiconductor nanoparticles, which can produce quantum size effect due to electron–hole recombination. The UV visible absorption spectrum of semiconductor nanoparticles depends on their size and the absorption maximum decreases with the nanoparticle size (Calandra et al. 1999). The UV–Vis absorption spectra of undoped and Ce^{3+}-doped ZnS nanocrystals are shown in Fig. 2. The absorption peaks were observed around 294 and 298 nm corresponding to pure ZnS and ZnS: Ce^{3+}, respectively. Since the absorption of Ce^{3+}-doped ZnS shifted to longer wavelength compared to undoped ZnS, cerium might be covalently bonded to ZnS (Jayavel et al. 2010). This prediction also supports the small shift in 2θ of the XRD pattern of Ce^{3+}-doped ZnS compared to that of undoped ZnS, as discussed earlier. The shift of the absorption edge to the longer wavelength side has been attributed to the strong exchange interactions between the d electrons of cerium and the s and p electrons of host band. On the other hand, when we studied the optical absorption for various concentrations of cerium, the peak position has no major change with doping concentrations. However, the absorption peaks of undoped and Ce^{3+}-doped ZnS are considerably blue-shifted compared to that of bulk phase ZnS (340 nm). This absorption shift is due to quantum size effect, representing a change in band gap along with exciton features, which can be used as a measure of particle size and size distribution (Laura Beecroft and Christopher 1997). The band gap energy of the nanocrystals was calculated from a simple energy wave equation. $E = hc/\lambda$ and the determined values are 4.22 and 4.16 eV for undoped and Ce^{3+}-doped ZnS, respectively. This result reveals that the size of the ZnS nanocrystals has been increased on doping.

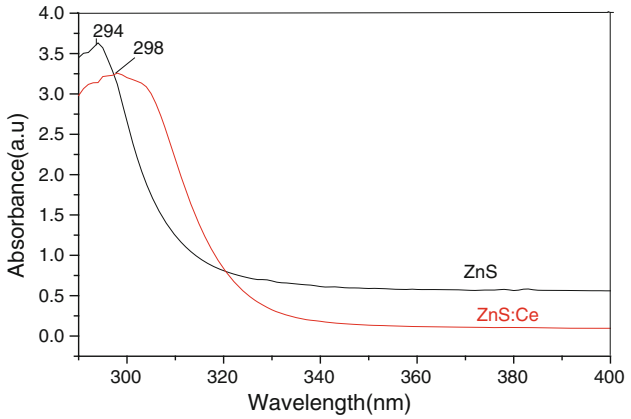

Fig. 2 UV–visible absorption spectra of ZnS and Ce^{3+}-doped ZnS nanorods

PL-measurement

PL Spectra were recorded at room temperature with 290 nm excitation. PL spectra of cubic ZnS and Ce^{3+}-doped ZnS nanocrystals are shown in Fig. 3. The PL spectrum of ZnS nanocrystals exhibits a sharp blue emission band located at 498 nm. This blue emission at 498 nm could be attributed to a recombination of electrons at sulfur vacancy donor level with holes at the zinc vacancy acceptor level (Murugadoss et al. 2011). However, on Ce^{3+} doping blue emission of ZnS has been completely quenched and two emission peaks centered at 356 and 607 nm are generated due to the 5d → 4f transition in Ce^{3+} ions (Grabmaier and Blasse 1994). Quenching of the ZnS emission and enhancement of the Ce^{3+} emission demonstrates that ZnS nanocrystals absorbed energy from the excitation source and transferred it nonradiatively to luminescent centers (Ce^{3+} ions).

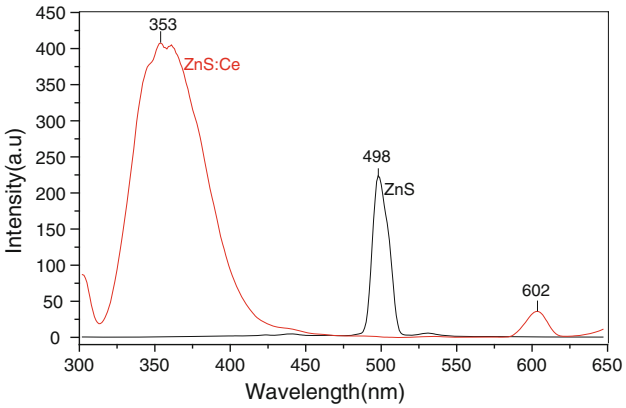

Fig. 3 PL spectra of ZnS and Ce^{3+}-doped ZnS nanorods

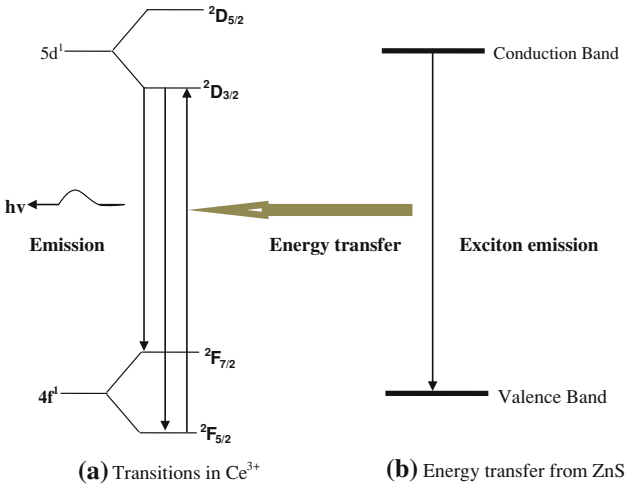

Fig. 4 Possible transitions in Ce^{3+} and mechanism of energy transfer from ZnS nanocrystals

The possible energy transfer mechanisms are show in Fig. 4a, b. The $5d^1$ excited configuration in Ce^{3+} is split by the crystal field into two components ($2D_{5/2}$ and $2D_{3/2}$), and the $4f^1$ ground state configuration yields two components ($2F_{5/2}$ and $2F_{3/2}$) due to spin-orbit coupling. The Ce^{3+} emission emanates from the lowest crystal field component of the $5d^1$ configuration to the two levels of the ground state. Since the blue emission from ZnS results from recombination in the ZnS, in this model, energy transfer is faster than hole trapping and recombination with electrons, therefore the blue emission from ZnS is quenched and emissions from Ce^{3+} are enhanced. This is shown in Fig. 4a, b where band gap excitation of ZnS has resulted in creation of an exciton, and subsequent nonradiative recombination results in excitation from the ground 4f states to the excited 5d states on the Ce^{3+} centre. Subsequent radiative relaxation on the Ce^{3+} would result in emissions at 356 and 607 nm.

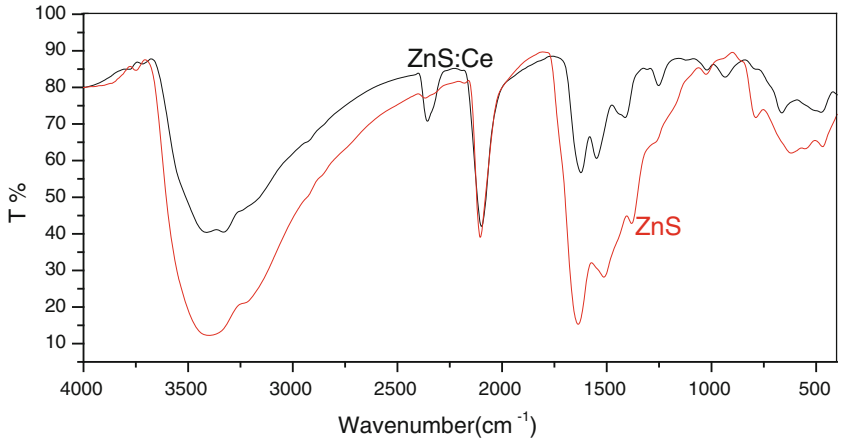

Fig. 5 FT-IR spectra of **a** undoped ZnS, and **b** Ce^{3+}-doped ZnS nanorods

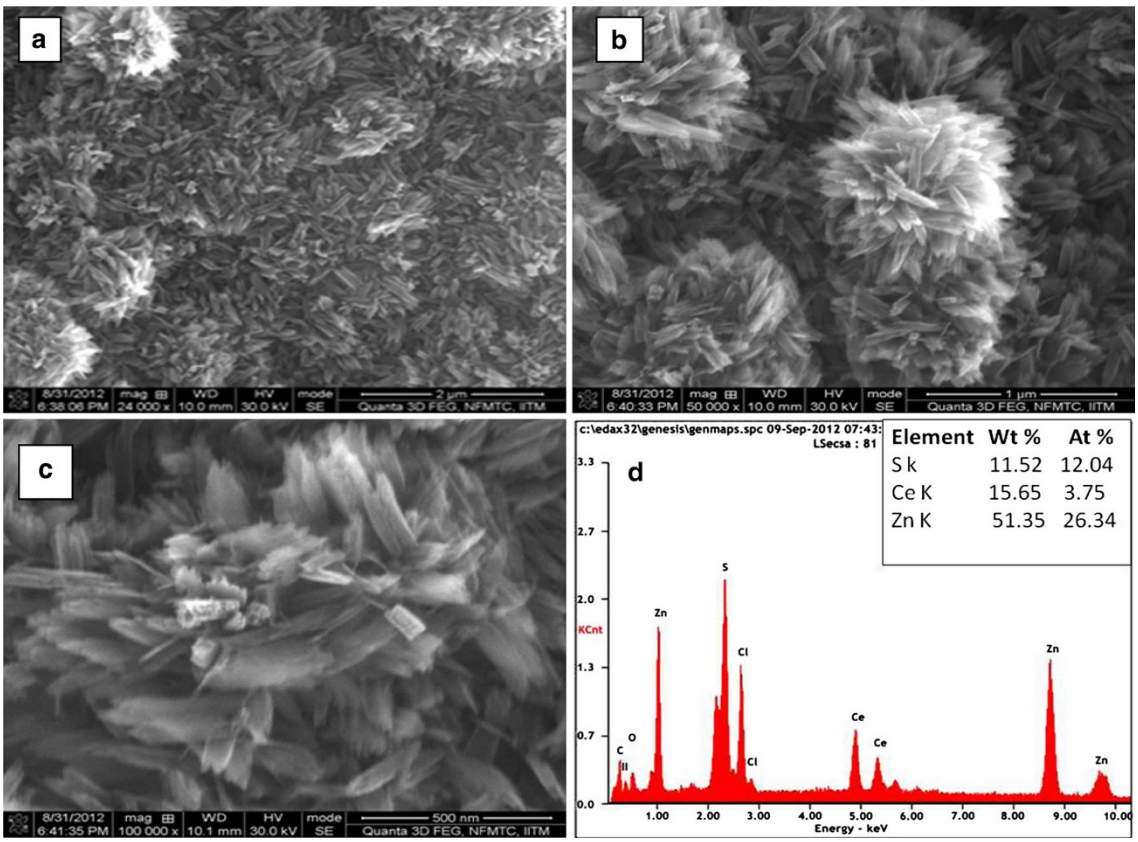

Fig. 6 **a–c** FESEM images of cerium-doped flowerlike ZnS nanorods, and **d** EDS spectrum of cerium doped ZnS

FT-IR study

Figure 5 depicts the FTIR transmission spectra of (a) undoped, and (b) Ce^{3+}-doped ZnS nanocrystals. The FTIR spectra of undoped and doped ZnS nanocrystals show a broad absorption peak in the range of 3,400 cm^{-1}, which is assigned to O–H stretching vibrations of absorbed water on the ZnS surface. The existence of this band can be attributed to the absorption of some atmospheric water during FT-IR measurements (Ramasamy et al. 2012). The bands at 1,500–1,650 and at 2,370 cm^{-1} are due to the C=O stretching mode arising from the absorption of atmospheric CO_2 on the surface of the nanoparticles (Qadri et al. 1999). Peaks appearing at 2,365 and 1,635 cm^{-1} are due to microstructure formation of the samples. In addition, the Zn–S vibration peak observed at 618 cm^{-1} in ZnS curve has been shifted to 660 cm^{-1} as a result of doping. Likewise, the peak at 1,381 cm^{-1} of ZnS is split into two peaks at 1,251 and 1,411 cm^{-1} for cerium-doped ZnS.

Morphological studies

Figure 6a–c shows typical field-emission scanning electron microscopy (FESEM) images of the cerium-doped ZnS nanocrystals. Figure 6b shows the aggregate of nanorods and the aggregate is actually flower-shaped structure with multiple petals. All the petals are joined together through their bases in such a way that the flower exhibits a spherical shape. Each petal of this flower-shaped structure is about 24–26 nm in diameter, and about 120–130 nm in length. To evaluate the elemental composition of as synthesized nanorods, the EDS analysis was carried out and the result is given in Fig. 6d. In EDS spectrum, numerous well-defined peaks were predicted to Zn, S, and Ce which clearly indicate that the synthesized nanorods are cerium-doped ZnS. The morphology and structure of ZnS nanorods were characterized in further detail by HRTEM and SAED. The HRTEM images of as synthesized rods with different magnifications and the SAED pattern are shown in Fig. 7a–d.

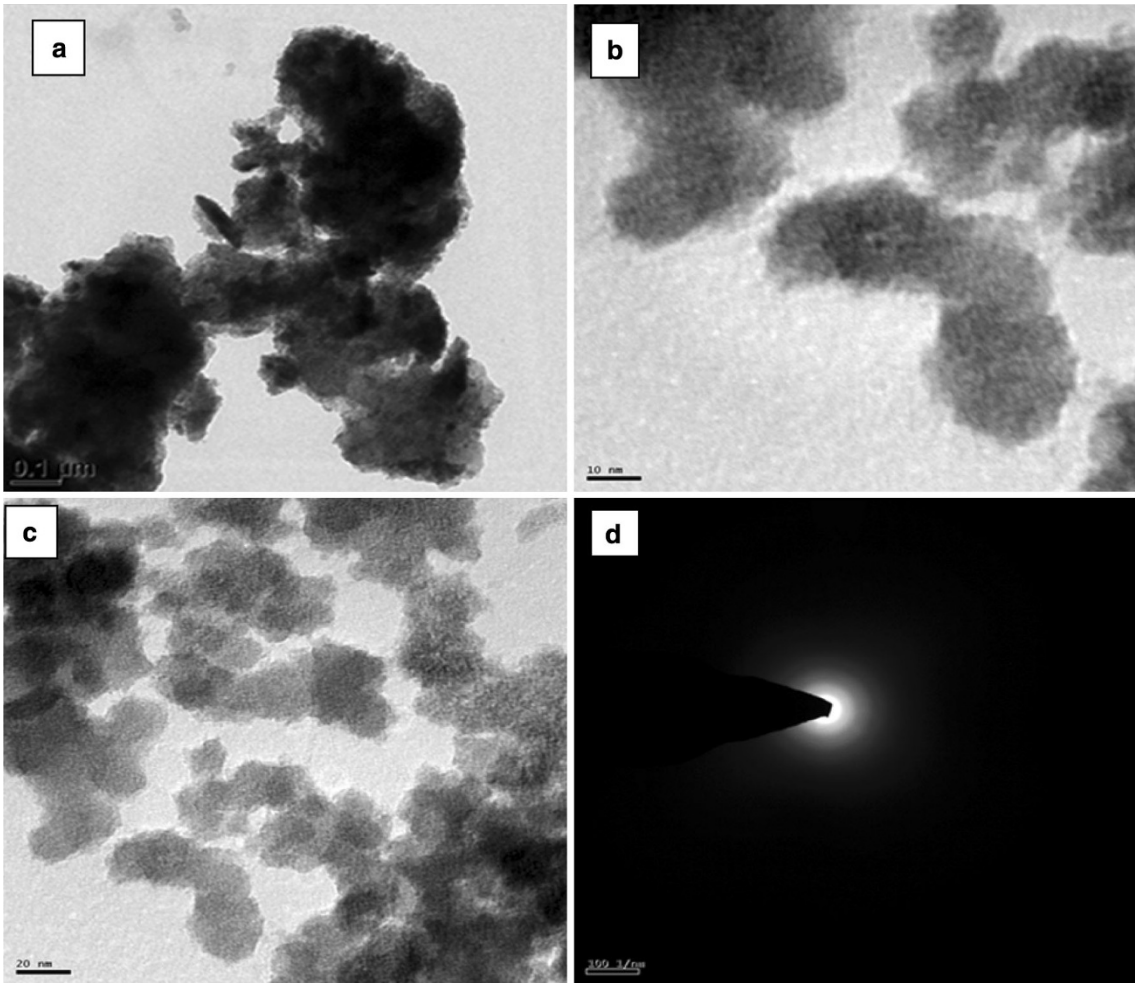

Fig. 7 **a–c** HRTEM images, and **d** SAED pattern of Ce^{3+}-doped ZnS nanorods

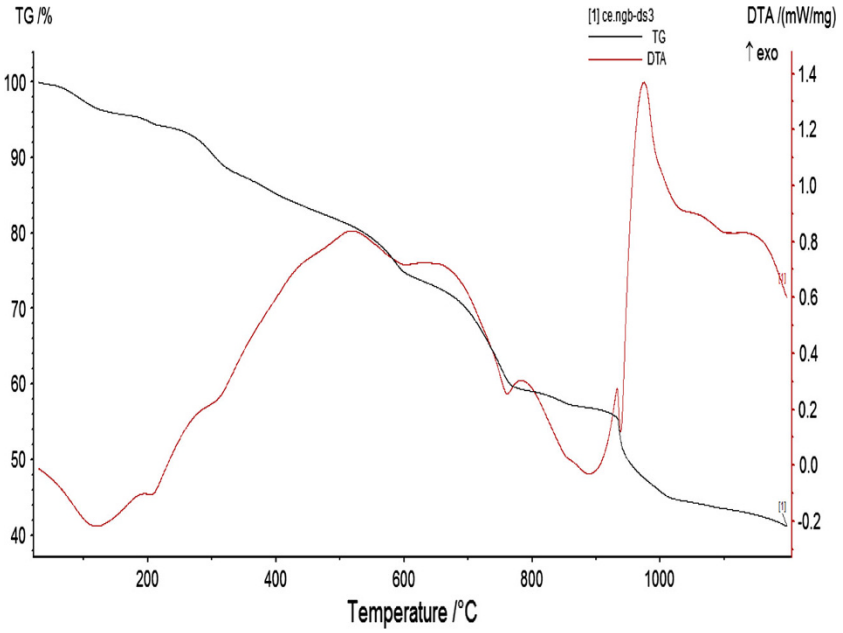

Fig. 8 TG-DTA curves of Ce^{3+}-doped ZnS nanorods

From the figure, it is observed that ZnS nanocrystals composed of uniform nanorods with average diameter of 22 nm and length of 140 nm were obtained. This is in good agreement with the size obtained from FESEM and XRD analyses. The structure of the grown rods was revealed by the selected area electron diffraction (SAED) pattern (Fig. 7d). The SAED pattern shows three rings corresponding to (111), (220), and (311) planes, respectively, which is in agreement with the XRD patterns.

TG–DTA analysis

The TG–DTA thermograms were recorded for ZnS: Ce^{3+} nanocrystals in the temperature range from room temperature to 1,200 °C with an interval of 20 °C/min in an air atmosphere. Figure 8 represents the combined plots of TG and DTA. From the TGA curve, it is noted that the weight loss of the nanocrystals are found to take place up to 1,020 °C. On the DTA curve seven endothermic peaks (110, 210, 310, 600, 750, 890, and 930 °C) and an exothermic peak (990 °C) were found in the heating process. The endothermic peaks at 110 and 210 °C are due to the removal of physically adsorbed water and chemically adsorbed water. The endothermic peak at 310 °C may be due to removal of organic matters. The endothermic peak found at 600 °C is due to valence variation of cerium. The strong endothermic peak at 750 °C can be associated with the removal of cerium. The well-established endothermic peak with maximum at 880 °C may be due to phase transformation. The final endothermic peak at 930 °C could be due to oxidation of ZnS to ZnO according to the following chemical equation.

$$2ZnS + 3O_2 \rightarrow 2ZnO + 2SO_2$$

To confirm the ZnO formation, the nano ZnS was annealed to 1,000 °C and then XRD was taken. The XRD pattern revealed the presence of hexagonal wurtzite ZnO with a very weak peak related to cubic ZnS (Figure not shown). In addition, above 1,100 °C, there is a sudden downtrend in DTA curve with significant weight loss. This may be due to release of residual sulfur ions from the sample.

Conclusions

We have synthesized Ce^{3+}-doped ZnS nanorods with flowerlike structure for the first-time using simple chemical precipitation method. The substitution of parts of lattice Zn of ZnS by Ce^{3+} ions is confirmed by XRD and EDS techniques. The doping of Ce^{3+} ions has tuned the band gap and photo luminescent properties of ZnS nanorods. The absorption edge of Ce^{3+}-doped ZnS nanorods was shifted to lower energy side relative to that of undoped ZnS. Undoped ZnS exhibits an emission maximum at 498 nm, whereas on doping two peaks, one at 356 nm and another at 604 nm, were obtained as a result of 5d → 4f transition in Ce^{3+} ions. Morphological features indicated that the Ce^{3+}-doped ZnS nanocrystals were composed of mono dispersed nanorods with flowerlike structure. The doping of Ce^{3+} enhanced the UV-emission efficiency of nanocrystalline ZnS. The thermograms have confirmed the stability of the synthesized products.

Acknowledgments The authors wish to thank Dr. S. Barathan, Professor and Head, Department of Physics, for providing necessary facilities to carry out this work. We also like to thank Dr. S. T. Balasubramaniyam, Director CAS in Marine Biology, Dr. S. Vijayalakeshmi, Scientist, COMAPS project and Dr. N. Krishnakumar, Assistant Professor, Department of Physics, Annamalai University, for their stimulating discussions during the period of this work.

References

Ageeth AB, Andries M (2001) Luminescence of nanocrystalline ZnS:Pb^{2+}. Phy Chem Chem Phys 3:2105–2121

Bando Y, Fang S, Shen GZ, Ye CH, Gautam UK (2007) Ultrafine ZnS nanobelts as field emittersX. Adv Mater 19:2593–2596

Bhargava RN (1996) Doped nanocrystalline materials-physics and applications. J Lumin 70:85–94

Calandra P, Goffredi M, Turco Liveri V (1999) Study of the growth of ZnS nanoparticles in water/AOT/n-heptane microemulsions by UV-absorption spectroscopy. Coll Surf A 160:9–13

Fang XS, Shen GZ, Golberg D (2007) Enhanced field-emission performance of ZnO nanorods by two alternative approaches. J Phys Chem 111:12673–12676

Fang XS, Bando Y, Liao MY, Gautam UK, Zhi CY, Dierre B, Sekiguchi T, Koide Y, Golberg D (2009) Single-crystalline ZnS nanobelts as ultraviolet-light (UV) sensors. Adv Mater 21: 2034–2039

Grabmaier BC, Blasse G (1994) Luminescent Materials. Springer, Berlin

Hu H, Zhang W (2006) Synthesis and properties of transition metals and rare-earth metals doped ZnS nanoparticles. Opt Mater 28:536–550

Jayavel R, Mohan R, Vijai Anand K (2010) Controlled synthesis and charactrization of cerium doped zns nanoparticles in HTMA matrix. Int J Nano Sci 10:487–493

Kim MR, Chung JH (2009) Spectroscopy and dynamics of Mn^{2+} in ZnS nanoparticles. Phys Chem Chem Phys 11:1003–1006

Laura Beecroft L, Christopher Ober K (1997) Nanocomposite Materials for Optical Applications. Chem Mater 9:1302–1317

Manzoor K, Vadera KSR, Kumar SRN (2004) Multicolor electroluminescent devices using doped ZnS nanocrystals. Appl Phys Lett 84:284–286

Murugadoss G, Rajamannan B, Ramasamy V (2011) Photoluminescence properties of monodispersed Mn^{2+} doped ZnS nanoparticles prepared in high temperature. J Mol Struct 991:202–206

Qadri SB, Skelton EF, Hsu D, Yang J, Gray HF, Ratna BR (1999) Size-induced transition–temperature reduction in nanoparticles of Zns. Phy Rev B 60:9191–9193

Ramasamy V, Praba K, Murugadoss G (2012) Study of optical and thermal properties in nickel doped ZnS nanoparticles using surfactants. Superlatt Microstruct 51:699–714

Torimoto T, Okazaki T, Sakuraoka M, Adachi T (2007) Facile synthesis of ZnS–AgInS2 solid solution nanoparticles for a color-adjustable luminophore. J Am Chem Soc 129:12388–12389

Wang MX, Fan XY (2006) Hydrothermal synthesis of single-crystal ZnS nanowires. Appl Phys A 84:409–412

Yu YL, Huang P, Lin H, Shan ZF (2010) Color-tunable luminescence for Bi^{3+}/Ln^{3+}:YVO_4 (Ln = Eu, Sm, Dy, Ho) Nanophosphors excitable by near-ultraviolet light. Phys Chem Chem Phys 12:7775–7778